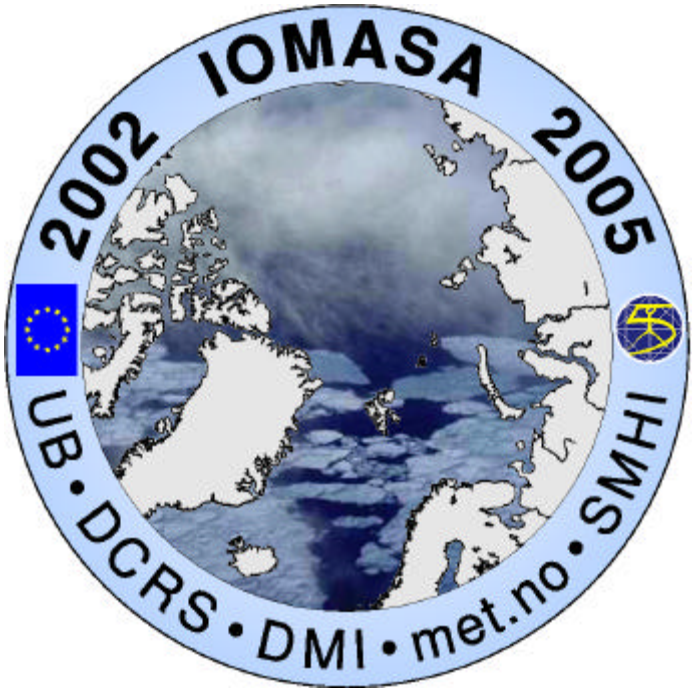

Report for IOMASA deliverable 4.2

Notes:
The following DMI scientific report constitutes IOMASA deliverable report 4.2. It documents performances of several ice concentration algorithms from a theoretical perspective. Final validation and possible adjustment of the results is pending the outcome of the IOMASA validation activities and will be reported in deliverable 4.4. Algorithm source code can be obtained on request.

Danish Meteorological Institute
Ministry of Transport

Scientific Report 04-03

Modelled radiometer algorithm ice concentration sensitivity to emissivity variations of the Arctic sea ice snow cover

Rasmus T. Tonboe & Søren Andersen

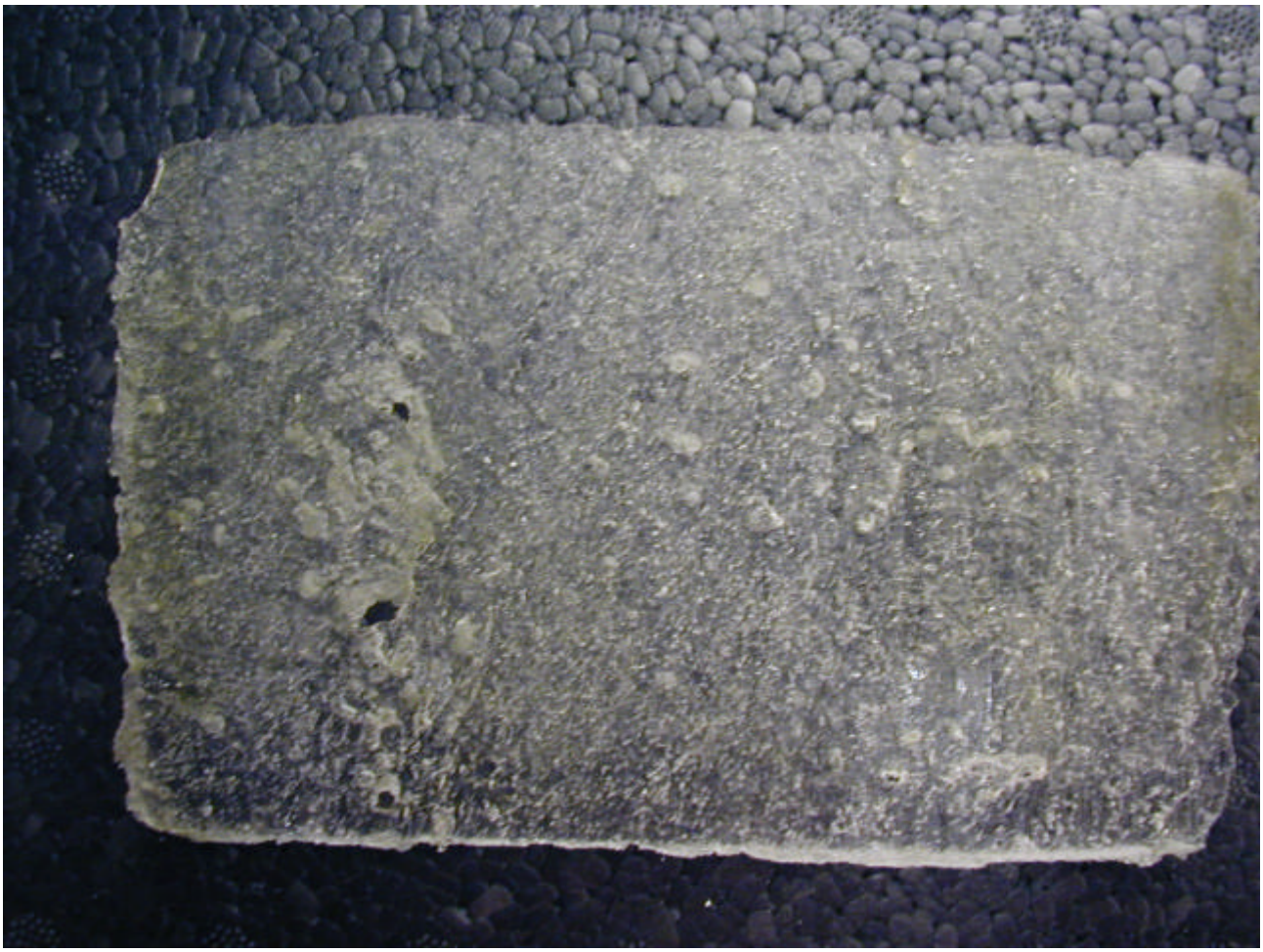

Ice sample Greenland Sea 2003/03/19, photo C. Haas.

Copenhagen 2005

Colophon

Serial title:
Scientific Report 04-03

Title:
Modelled radiometer algorithm ice concentration sensitivity to emissivity variations of the Arctic sea ice snow cover

Subtitle:

Author(s):
Rasmus T. Tonboe & Søren Andersen

Other contributors:

Responsible institution:
DMI

Language:
English

Keywords:
sea ice, ice concentration algorithms, microwave emission modelling

Url:
www.dmi.dk/dmi/sr04-03

Digital ISBN:
87-7478-504-4

ISSN:

Version:

Website:
www.dmi.dk

Content:

Abstract

The snow microwave emission model MEMLS, extended to include the emission from sea ice, is used to test the sensitivity of nine different ice concentration algorithms to snow microphysical and emissivity variability.

Resumé

Sne mikrobølge-strålingsmodellen MEMLS, udviddet til at inbefatte strålingen fra havis, anvendes til at vurdere ni forskellige iskoncentrationsalgorithmers følsomhed overfor sneens emissivitet og mikrofysiske egenskaber.

Preface

DMI's obligation in the EU 5th framework programme project IOMASA is formulated in the second objective: "*improved remote sensing of sea ice with more accurate and higher resolved ice concentrations*". The present report describes an investigation of the computed sea ice concentration and its simulated sensitivity to the emissivity of snow cover on sea ice using a microwave emission model. Nine different ice concentration algorithms have been investigated. The Microwave Emission Model for Layered Snow-packs (MEMLS) developed by Wiesmann & Mätzler (1999) for snow on land is well documented and validated. An extended version of MEMLS, which includes emission from sea ice, has been developed within the IOMASA project. The extended emission model is not validated for snow cover on sea ice and this report is not attempting a validation or assessing the accuracy of the sea ice module. We admit that validation is very important for confidence in the results, but we are not in possession of a validation data set.

An earlier IOMASA report (Tonboe et al., 2003) concluded, based on observations, that the computed sea ice concentration using passive microwave data may be biased by changes in the snow and sea ice emissivity. The present report elaborates this work with more emphasis on emission theory. It is part of an ongoing effort in the IOMASA project to improve the sea ice concentration estimate. This report is a DMI contribution to the IOMASA project.

1. Introduction

"…a thick slab of Arctic pack ice reduces the wintertime sensible heat loss from ocean to atmosphere by a factor of 100 to 1000, compared to fluxes from open water." (Moritz, 1988, p. 1). Even small changes in the sea ice concentration thus have a significant impact on energy fluxes between the ocean and the atmosphere. Therefore, ice concentration is an important ice cover parameter and must be estimated accurately (Steffen & Schweiger, 1991). Mean accuracy of some of the more common algorithms, used to compute it from SSM/I data, such as NASA Team (Cavalieri et al., 1984) and Boot-strap (Comiso, 1986) are reported to be 1-6 % in winter (Steffen & Schweiger, 1991; Emery et al., 1994; Belchansky & Douglas, 2002).

Each of the algorithms may perform better under certain conditions (Emery et al., 1994). Their sensitivity to emissivity and thermometric temperature of the target depend on the selection of Tb at different polarisations and frequencies (Comiso et al., 1997). Recent validation results suggest that in general Boot-strap ice concentration is more seasonally robust than the NASA Team ice concentration estimate (Belchansky & Douglas, 2002).

The computed ice concentration accuracy is further degraded by particular atmospheric constituents like cloud liquid water, where NASA Team ice concentration erroneously can increase by 10 % (Oelke, 1997), and changes in the ice emissivity, where the computed concentration can be depressed by 20 % (Tonboe et al., 2003). The sensitivity of the different ice concentration algorithms e.g. NASA Team, Boot-strap and near 90 GHz (Svendsen et al., 1987) to the atmosphere or ice brightness temperature is not the same (Andersen et al., 2003; Tonboe et al. 2003). In order to asses and increase accuracy of the computed ice concentration, this report is investigating ice concentration computed using nine different radiometer algorithms and its sensitivity to changes in the snow cover properties such as density, layering and grain size using a microwave emission model. The emission model is an extended version of MEMLS (Wiesmann & Mätzler, 1999) that treats the emission from layered snow as well as sea ice. Tonboe et al. (2003) show that the problem with the changing ice emissivity is most abundant close to the ice edge where warm air is frequently advected over the ice causing ice surface melt and snow and ice metamorphosis. However, during a period of three winters (2000-2003) there were about 10 cases of surface melt >100 000 km^2 penetrating deep into the seasonal and perennial ice cover in Baffin Bay, Barents Sea and central Arctic Ocean (Tonboe et al., 2003). These events and in general the variable sea ice emissivity constitute a significant problem because the emissivity change of the snow and ice is persistent and difficult to detect.

In this report MEMLS is used for a sea ice related sensitivity study, however emissivity models have potential in atmospheric remote sensing as well: satellite passive microwave data is used for measuring atmospheric constituents such as cloud liquid water and water vapour, which are assimilated in atmospheric numerical models. In order to decrease the measurement error of these atmospheric constituents it is necessary to get a good estimate of the surface emissivity. Emissivity models represent an important interpolation and extrapolation tool for obtaining a surface emissivity estimate at e.g. the water vapour absorption frequencies.

2. Snow and sea ice emission modelling

The dielectric properties of snow are determined mainly by the density and wetness (Ulaby et al., 1986). The dielectric constant of snow is affecting the reflection and transmission coefficients and the absorption coefficient. Scattering in the snow pack becomes important for large snow grains or high frequency (Mätzler, 1987). The dielectric properties of sea ice are to a large extent given by the brine and air-inclusion volume (Shokr, 1998). Important for scattering in sea-ice is the size and density of brine pockets or air bubbles (Winebrenner et al. 1992).

Important radiative processes in a homogeneous snow layer can be described using simple radiative models (Ulaby & Stiles, 1980; Mätzler, 1987). However, snow cover on land, ice or sea-ice is a layered medium and therefore the simple models fail to simulate observations by not accounting for important reflections between layers (Surdyk & Fily, 1993; Wiesmann & Mätzler, 1999). Winebrenner et al. (1992) gives a review of different types of emission models that exist for sea-ice. One of the more sophisticated models based on Many Layer Strong Fluctuation Theory (MLSFT) represents the sea ice module in the MicroWave MODel (MWMOD) described by Fuhrhop et al. (1997).

MWMOD is a combined atmosphere, ocean and sea-ice radiometer model. The snow and sea-ice model theory is presented in Winebrenner et al. (1992) and applied in Fuhrhop et al. (1998) and Johnson & Heygster (2000). The simulated emissivity is dictated by volume scattering for electrically dense scatterers and coherent reflections between layers with dielectric contrast (Stogryn, 1986; Winebrenner et al., 1992). Details are given in the references above. The sea ice module was tested in a previous IOMASA report by Tonboe et al. (2003) and it largely failed to reproduce the observed emissivity realistically. Similar experiences with a comparable strong fluctuation theory model for snow packs lead Wiesmann & Mätzler, (1999) to develop the Microwave Emission Model for Layered Snow-packs (MEMLS). MEMLS has been tested and validated for snow-cover on land with satisfactory results. Here MEMLS has been extended to include emission from sea-ice. The model and modifications are described in the next section.

3. Overview of the changes made to MEMLS

"*A thermal microwave emission model of layered snow packs (MEMLS) was developed for the frequency range 5-100GHz. It is based on radiative transfer, using six-flux theory to describe multiple volume scattering and absorption, including radiation trapping due to total reflection and a combination of coherent and incoherent superpositions of reflections between layer interfaces. The scattering coefficient was determined empirically from measured snow samples, whereas the absorption coefficient, the effective permittivity, refraction and reflection at layer interfaces were based on physical models and on measured ice dielectric properties. … A limitation of the empirical fits and thus of MEMLS is in the range of observed frequencies and correlation lengths (a measure of grain size).*" (Wiesmann & Mätzler, 1999). The model is using snow quantities and structure i.e. sequence of layers, density, correlation length, temperature, moisture. In order to apply this model to compute the emission of both snow and sea ice it is necessary to include modules that compute the dielectric properties, and scattering of sea ice. In first-year sea-ice the dominant scatterers are the small liquid brine inclusions also called brine pockets. The dielectric constant of liquid brine is an order of magnitude larger than the solid ice. The dielectric constant of first-year sea ice is therefore primarily a function of brine volume. Before the dielectric constant and the scattering coefficient of sea ice can be computed it is necessary to compute some important properties of the brine solution. These properties are computed using the models in Ulaby et al. (1986) appendix E:

- Volume of brine, a function of temperature and salinity of sea ice.
- Salinity of brine, a function of temperature.
- Normality of brine, a function of the salinity of brine.
- Conductivity of brine, a function of temperature and normality.
- Relaxation time of the brine solution, a function of temperature and normality.
- Static dielectric constant of brine, a function of temperature and normality.
- Dielectric constant of brine, a function of EM frequency, static dielectric constant, relaxation time, and conductivity of brine.

The dielectric constant of sea ice is computed using Polder - Van Santen mixing formulas. We follow the recommendations of Shokr (1998), i.e. the dielectric constant of multi-year (MY) ice is a mixture of any shape (spheres are used) of air inclusions in ice. The dielectric constant of first-year (FY) ice is a function of the dielectric constant of pure ice, shape/orientation, volume and dielectric constant of the brine pockets (spheres are used).

The scattering in sea ice is computed using the improved born approximation (Mätzler, 1998). Air-inclusions are scatterers in MY ice and brine pockets in FY ice. The scattering coefficient is in general a function of: dielectric constant of pure ice, dielectric constant of brine or air, dielectric constant of the sea ice mixture, volume of brine or air, EM frequency and correlation length of scatterers (measure of scatter size and distribution, see e.g. Mätzler, 2002).

These additional modules are then included in the model computation scheme. The focus of the sensitivity study is on first-year ice.

The MEMLS code is written in MATLAB. With a few minor changes, this sea ice version of MEMLS is now running in the free-software programme OCTAVE (www.octave.org).

4. In situ and satellite data

Sea ice in situ data were collected in Fram Strait during the CRYOVEX campaign 2003/ R/S Polarstern cruise by Christian Haas, Alfred Wegener Institute. Coincident satellite AMSR radiometer data were collected by Leif Toudal, Technical University of Denmark.

4.1. In situ snow and ice profiles

The snow and ice profile data contained information on vertical temperature, salinity and a short description of the snow cover. Density and correlation length was then estimated before the data could be used as input to MEMLS (see e.g. Mätzler, 2002). Two first-year ice profiles were collected 23/03/2003 on position 76.26N, 23.28E one with a thick snow cover (36cm) and one with thin snow cover (7cm). The input data from these two profiles are shown in table 1 and 2 respectively.

Layer #	T[K]	Density[kg/m3]	Thickness[cm]	PCI[mm]	S[psu]	Snow/Ice
1	251.1	400	14.0	0.05	0	Soft, fine grained wind slab
2	262.1	920	0.1	0.1	0	Thin icy layer
3	262.1	400	16.0	0.1	0	Hard wind slab
4	264.2	200	6.0	0.15	0	Icy depth hoar
5	264.7	920	5.0	0.17	13.6	Ice
6	263.8	920	10.0	0.17	11.3	Ice
7	261.9	920	10.0	0.17	8.5	Ice
8	261.6	920	8.5	0.17	7.1	Ice
9	261.0	920	7.0	0.17	7.7	Ice
10	260.7	920	8.5	0.17	8.0	Ice
11	263.1	920	10.0	0.17	7.5	Ice
12	264.8	920	10.0	0.17	4.4	Ice
13	265.1	920	10.0	0.17	4.0	Ice
14	265.8	920	10.0	0.17	3.2	Ice
15	267.1	920	10.0	0.17	4.8	Ice
16	269.2	920	10.0	0.17	5.8	Ice

Table 1. The ‘thick’ snow profile. Input data includes T, thermometric temperature, density, thickness, PCI, correlation length, S, salinity and a short description of the layer.

Layer #	T[K]	Density[kg/m3]	Thickness[cm]	PCI[mm]	S[psu]	Snow/Ice
1	253.0	400.0	4.0	0.05	0	Icy, hard depth hoar
2	256.0	150.0	3.0	0.15	0	Hard wind slab
3	259.0	920.0	4.5	0.17	13.5	Ice
4	259.4	920.0	9.0	0.17	10.7	Ice
5	260.3	920.0	10.5	0.17	8.5	Ice
6	261.6	920.0	11.5	0.17	5.8	Ice
7	262.3	920.0	10.5	0.17	8.5	Ice
8	263.7	920.0	12.5	0.17	10.9	Ice
9	265.6	920.0	11.5	0.17	4.8	Ice
10	266.1	920.0	8.0	0.17	5.3	Ice
11	266.7	920.0	11.5	0.17	4.7	Ice
12	268.1	920.0	13.0	0.17	4.4	Ice
13	269.2	920.0	11.5	0.17	5.4	Ice

Table 2. The ‘thin’ snow profile. Input data includes T, thermometric temperature, density, thickness, PCI, correlation length, S, salinity and a short description of the layer.

4.2. The AMSR radiometer data

The Advanced Microwave Scanning Radiometer (AMSR) is a total power radiometer measuring the up-welling brightness temperature from the Earths surface and atmosphere at 6 microwave frequencies and dual polarisation (v and h) at a constant 55º incidence angle. The swath width is about 1445 km and the frequencies and resolutions are summarised in table 3

(www.ghcc.msfc.nasa.gov/AMSR/).

Mean frequency [GHz]	6.9	10.7	18.7	23.8	36.5	89.0
Mean resolution [km]	56	38	21	24	12	5

Table 3. Mean resolution and frequency of AMSR.

The brightness temperatures are denoted Tb and the subscript indicate the frequency and polarisation e.g. Tb_{19v} for the brightness temperature measured at 19GHz (18.7GHz) and vertical polarisation.

5. MEMLS simulation results

The profile data in table 1 and 2 were used as input to MEMLS and the simulation results compared to coincident satellite AMSR radiometer data. Neither the thick or thin profile simulations matched the AMSR data completely at all frequencies. An artificial profile was therefore constructed using realistic properties for snow and ice. MEMLS simulations using the artificial profile matched the AMSR data at all frequencies. The artificial profile was used as a reference in a study of the sensitivity to snow properties of nine different radiometer ice concentration algorithms.

5.1. Comparison of AMSR data and the 'thin' and 'thick' snow cover MEMLS simulations

The MEMLS simulation of the 'thick' snow cover (input data in table 1) is shown in figure 1. While it reproduces the AMSR brightness temperatures at high frequencies, it fails to reproduce the horizontally polarised brightness temperatures in particular at low and intermediate frequency. Figure 2 shows the simulated brightness temperatures obtained from the thin snow cover profiles. Here the scattering is clearly too large and only vertically polarised brightness temperatures up to 36.5 GHz are reproduced reasonably well. These findings are not surprising given that the quite different snow profiles are observed within the same AMSR field-of-view; however, they stress the importance of dedicated validation data.

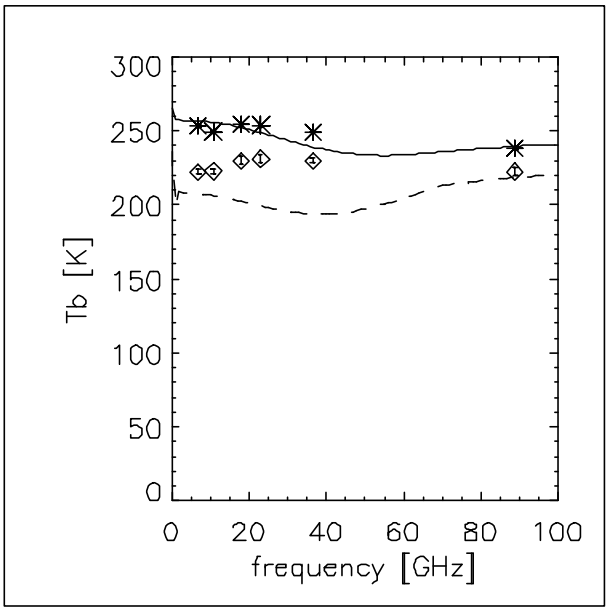

Figure 1. AMSR data on 23/03/2003 and MEMLS simulation using the 'thick' snow cover profile in table 1.

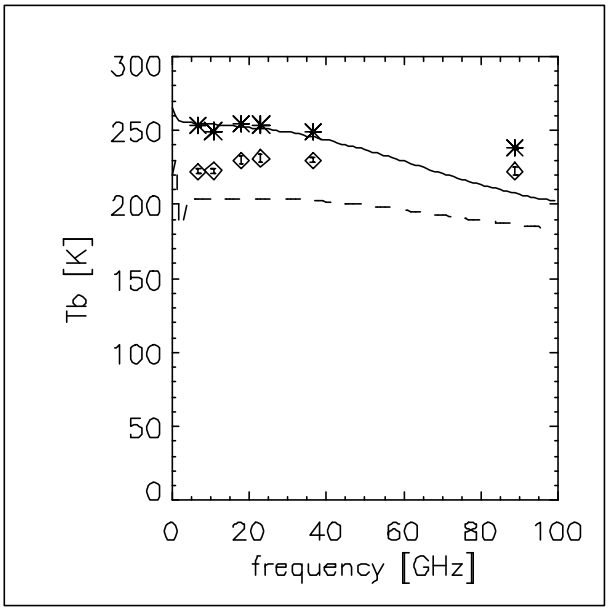

Figure 2. AMSR data on 23/03/2003 and MEMLS simulation using the 'thin' snow cover profile in table 2.

5.2. The artificial snow and ice profile

The artificial snow profile is constructed using realistic properties for snow and first-year ice. The properties are shown in table 4. The simulation using MEMLS is compared to AMSR measurements on 23/03/2003 in figure 3 & 4. The scattering in the snow is computed using an empirical fit. A constructed multi-year ice profile is shown in table 5. The simulation of this profile using MEMLS is shown in figure 5.

Type	T[K]	Density[kg/m3]	Thickness[cm]	PCI[mm]	S[psu]	Snow/ice
Nearly new snow	253.0	260	7.0	0.05	0	Snow
Hard densified slap	257.0	410	5.0	0.08	0	Snow
Coarse grains	261.0	320	1.0	0.14	0	Snow
FY sea ice	262.0	920	2.0	0.18	7.0	Ice
FY sea ice	262.5	920	100.0	0.15	5.0	Ice

Table 4. The constructed first-year ice profile used as input to MEMLS.

Type	T[K]	Density[kg/m3]	Thickness[cm]	PCI[mm]	S[psu]	Snow/ice
Nearly new snow	253.0	260	7.0	0.05	0	Snow
Hard densified slap	255.0	410	5.0	0.08	0	Snow
Coarse grains	257.0	320	1.0	0.14	0	Snow
MY sea ice	258.0	500	5.0	0.35	0.0	Ice
MY sea ice	260.0	700	5.0	0.29	0.0	Ice
MY sea ice	261.0	900	200.0	0.11	3.0	Ice

Table 5. The constructed multi-year ice profile used as input to MEMLS.

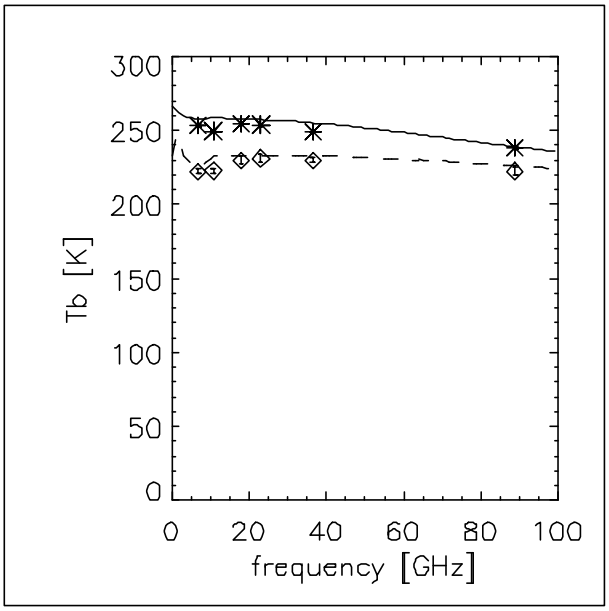

Figure 3. Comparison between AMSR data and MEMLS simulations using the input data in table 4 and an empirical scattering model.

The simulated Tb especially at high frequency (89GHz) is sensitive to the scattering model which is used. An empirical scattering model was used in figure 3. Figure 4 shows a simulation with the theoretical improved Born approximation scattering model for spherical scatters for comparison. In a natural snow cover there are both rounded and oblate snow grains and we therefore use the empirical fit for simulations in the following.

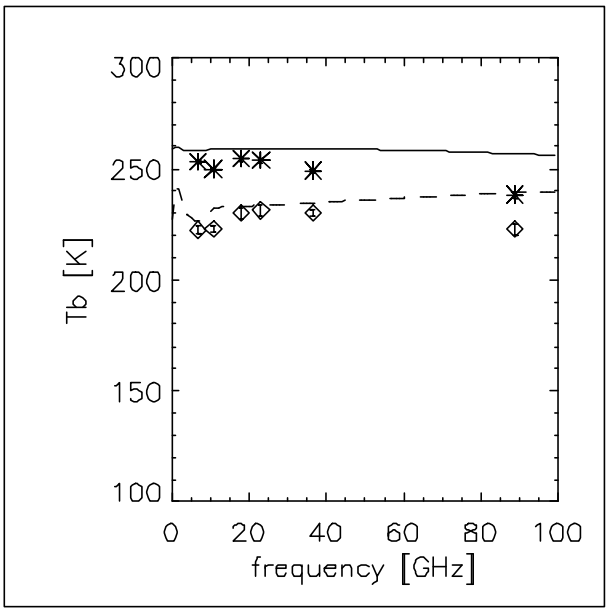

Figure 4. Comparison between AMSR data and MEMLS simulations using the input data in table 4 and the improved Born approximation scattering model.

Simulations using MEMLS and the constructed profile in table 5 as input is shown in figure 5. We note that Tb at medium and high frequency (>19GHz) is reduced due to scattering in the ice whereas the polarisation is similar to the first-year ice profile as expected. This can be taken as a sanity check of the first-year and multiyear ice modules.

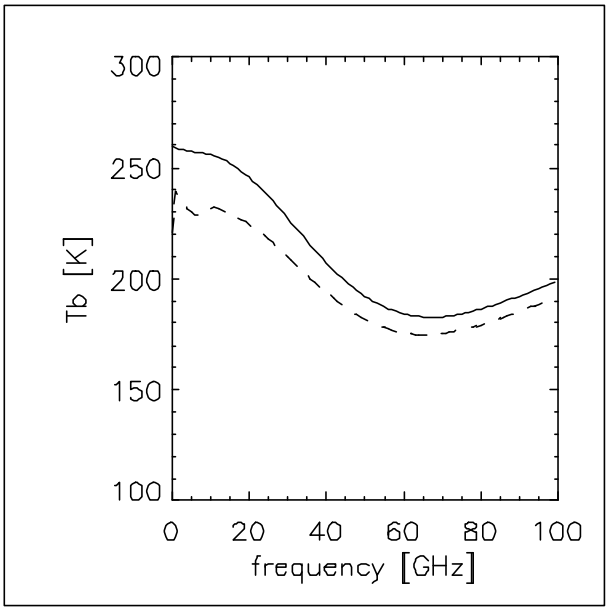

Figure 5. Simulated multi-year ice Tb using table 5 as input to MEMLS.

5.3. The simulated ice concentration sensitivity to snow emissivity

In the following, we simulate the sensitivity of nine different ice concentration algorithms to variations in the upper snow layer density and to correlation length in the bottom snow layer: NASA Team (Cavalieri et al., 1984), Comiso Boot-strap (frequency/polarisation mode) (Comiso, 1986), Near 90GHz (Svendsen et al., 1987), Bristol (Smith, 1996), Cal-val (Ramseier, 1991), NORSEX (Svendsen et al., 1983), TUD (Pedersen, 1998) and NASA Team2 (Markus & Cavalieri, 2000). The initial first-year ice profile, described in the table 4, is marked by 'R' in figures 6 to17. The upper snow layer density is varied between 100-410 kg/m^3, and the correlation length of the bottom snow layer between 0.14-0.32 mm. First-year ice tie-points were adapted from the reference simulation, to yield 100 % ice concentration for the reference profile. The remaining (multi-year ice and open water) tie-points were taken from the January tie-point set of Andersen (1999).

5.3.1. NASA Team algorithm

The NASA Team algorithm is exploiting the polarisation (PR) and gradient ratio (GR) differences between open water, old ice and first-year ice. The sensitivity to physical temperature is reduced when using the normalised PR and GR in equation 1 and 2 i.e.

$$PR_{19} = \frac{Tb_{19}^{v} - Tb_{19}^{h}}{Tb_{19}^{v} + Tb_{19}^{h}} \qquad (1).$$

The subscript 19 refer to the frequency in GHz and v and h refer to vertical and horizontal respectively.

$$GR_{19v/37v} = \frac{Tb_{37}^{v} - Tb_{19}^{v}}{Tb_{37}^{v} + Tb_{19}^{v}} \qquad (2).$$

The subscript 19 and 37 refer to the frequency in GHz and v refer to the vertical polarisation.

The NASA Team algorithm ice concentration sensitivity to variations in upper snow layer density and bottom snow layer correlation length is shown in figure 6. It is clear that the MEMLS simulations produce PR and GR that is quite close to the observed first-year ice tie-point value.

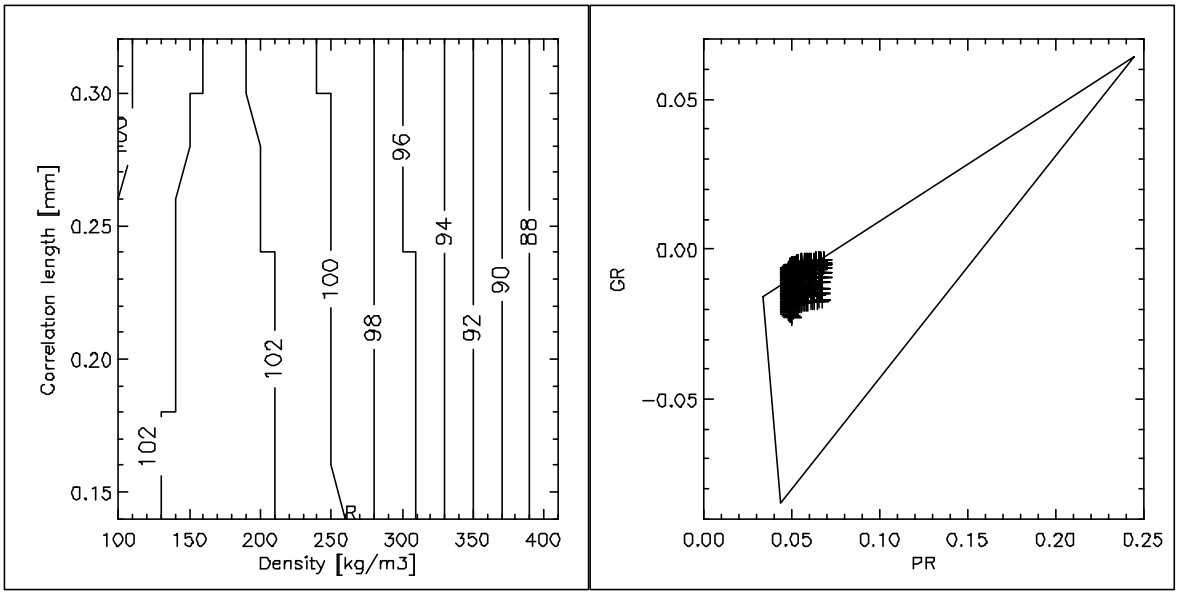

Figure 6. Simulated NASA Team algorithm sensitivity to variations in layering and grain size in the snow cover (left). Simulated data placed in the retrieval triangle based on Andersen (1999) (right).

Figure 7 show the simulated sensitivity of $GR_{19/37}$ and PR_{19} to the same parameters used to simulate the ice concentration sensitivity in figure 6. The minimum polarisation observed in the density interval between 150 and 200 kg/m^3 is the result of the competing effects:
1) reduced penetration through the upper snow layer and high air-snow contrast, and
2) deeper penetration and large density contrast between the two upper snow layers.

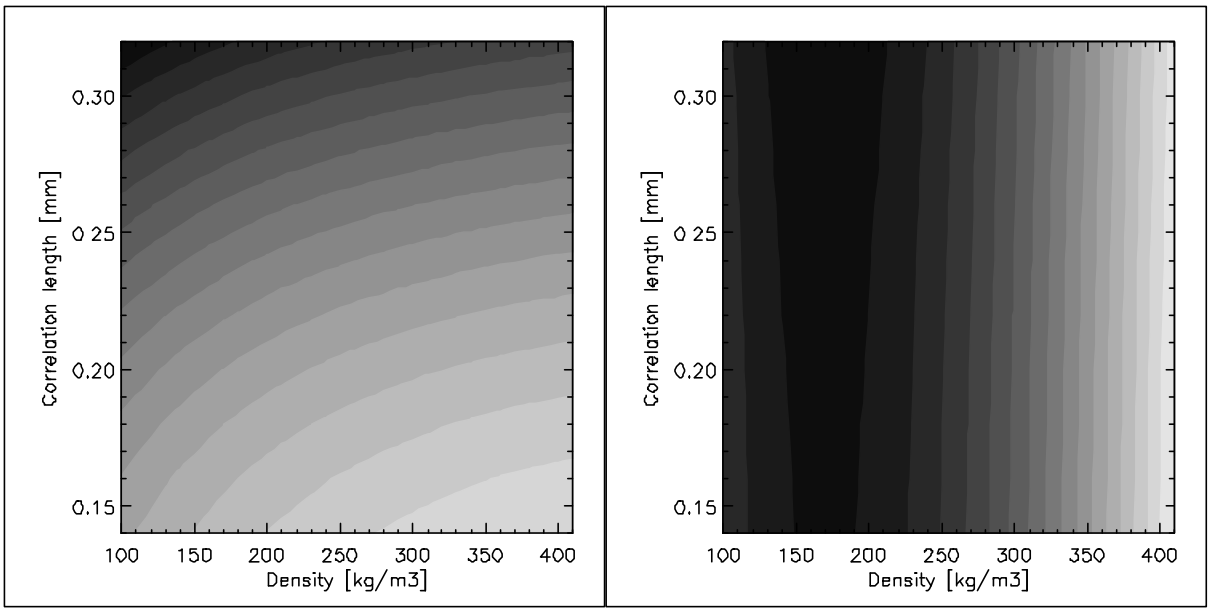

Figure 7. Simulated gradient ratio (left), values range from -0.023 to -0.004, and polarisation ratio (right), values from 0.048 to 0.068 for variations in layering and correlation length in the snow cover (bright values indicate higher values).

5.3.2. Comiso Boot-strap algorithm (frequency mode)

In Tb_{37v} Tb_{19v} space, consolidated ice forms a linear cluster separated from the open water cluster centred on a point. Sea ice cover at intermediate concentrations is in the space between open water and consolidated ice. The simulated sensitivity of the Comiso Boot-strap algorithm ice concentration to density of the upper snow layer and the correlation length of the bottom snow layer is shown

in figure 8.

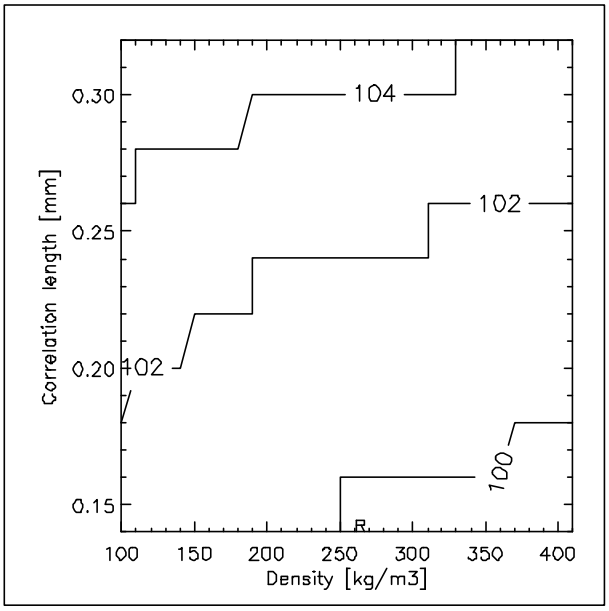

Figure 8. Simulated Comiso Boot-strap algorithm (frequency mode) sensitivity to variations in layering and grain size in the snow cover.

The simulated Tb_{19v} and Tb_{37v} used in the Boot-strap algorithm is shown in figure 9.

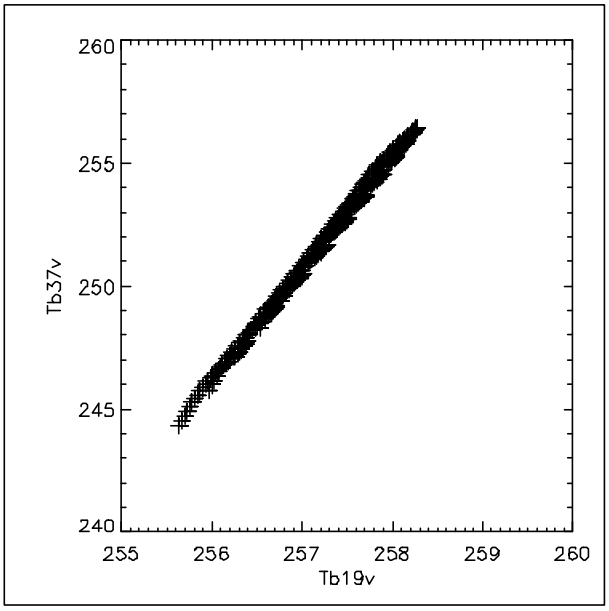

Figure 9. Simulated 19v and 37v brightness temperatures.

5.3.3. Near 90GHz algorithm

The 90 GHz ice concentration algorithm by Svendsen et al. (1987) uses the observation that the difference in emissivity between horizontal and vertical polarisation is small for first-year and multiyear ice types, but large for open water. The following formulations for the ice and open water cases are interpolated by a smooth function:

$$C_T = (1+\frac{b}{a})\frac{P}{P_1} - \frac{b}{a}, \quad C_T \to 1$$
$$C_T = (\frac{b}{a})\frac{P}{P_0} - \frac{b}{a}, \quad C_T \to 0 \qquad (1)$$

$P=T_B(85,v)- T_B(85,h)$ is the observed polarisation difference. The constants **a** and **b** depend on the ice and water tie points. P_1 and P_0 are observed polarisation differences over sea ice and open water to be estimated from the current orbit. P_1 is assumed to contain a smaller atmospheric influence than P_0, and thereby the interpolation step implies a low order atmospheric correction. In this study P_0 and P_1 are computed from the tie-points, implicitly disabling the atmospheric correction.

The simulated sensitivity to density of the upper snow layer and the correlation length of the bottom snow layer is shown in figure 10.

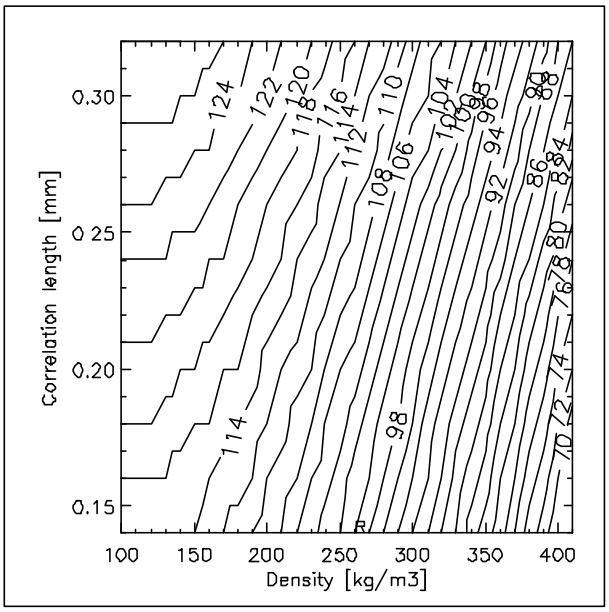

Figure 10. Simulated Near 90GHz algorithm sensitivity to variations in layering and grain size in the snow cover.

The high frequency polarisation difference is shown in figure 11.

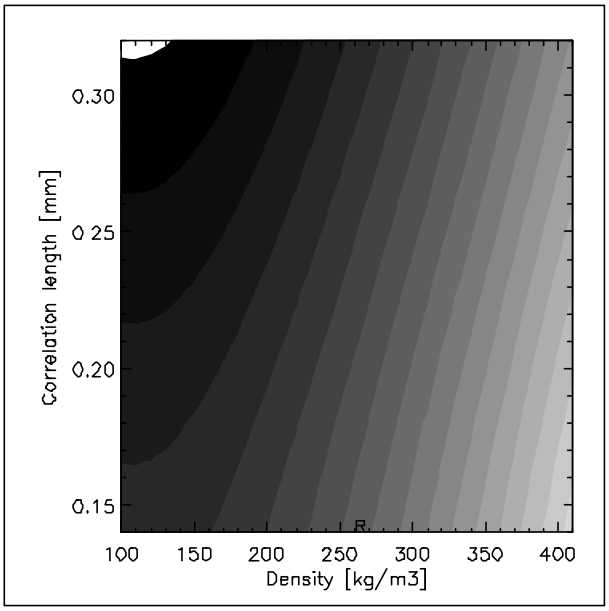

Figure 11. Simulated polarisation difference between Tb_{89v} and Tb_{89h} (bright values indicate higher values, range of values: 5.8K to 21.6 K).

5.3.4. Bristol algorithm

The Bristol algorithm is conceptually similar to the Boot-strap algorithm except the brightness temperature space used for ice concentration quantification has been transformed as a linear combination of Tb_{19v}, Tb_{37v} and Tb_{37h} to reduce noise. Its sensitivity to density of the upper snow layer and correlation length of the bottom snow layer, shown in figure 12.

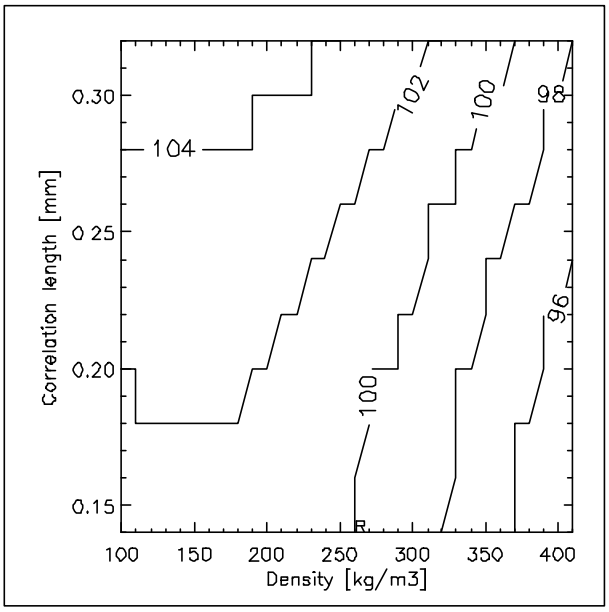

Figure 12. Simulated Bristol algorithm sensitivity to variations in layering and grain size in the snow cover.

5.3.5. Cal-val algorithm

The Cal-val algorithm quantifies ice concentration in terms of a linear combination of Tb_{37v} and Tb_{19v}. The brightness temperatures are not normalised and the algorithm is therefore sensitive to variations in the physical temperature. Figure 13 show the simulated sensitivity of Cal-val to density in the upper snow layer and correlation length in the bottom layer. The physical temperature is constant.

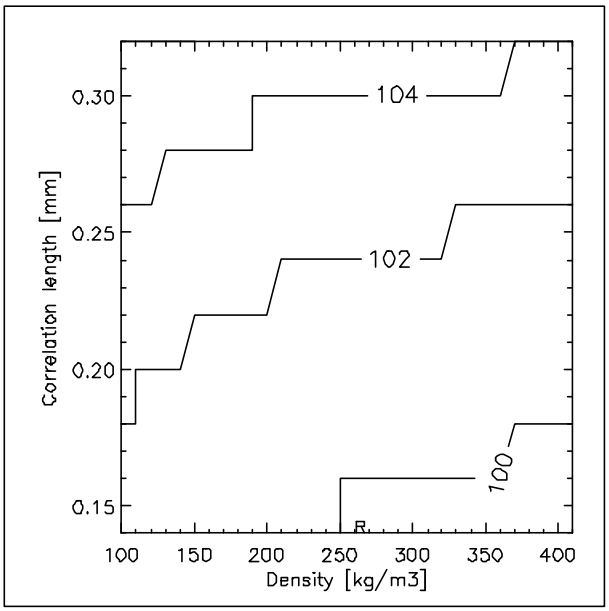

Figure 13. Simulated Cal-val algorithm sensitivity to variations in layering and grain size in the snow cover.

5.3.6. Comiso Boot-strap (polarisation mode)

The Comiso Boot-strap algorithm in polarisation mode is similar to the Comiso Boot-strap in frequency mode (section 4.3.2) except it is using Tb_{37v} and Tb_{37h} instead of Tb_{37v} and Tb_{19v}. Its sensitivity to density of the upper snow layer and correlation length in the bottom snow layer is shown in figure 14.

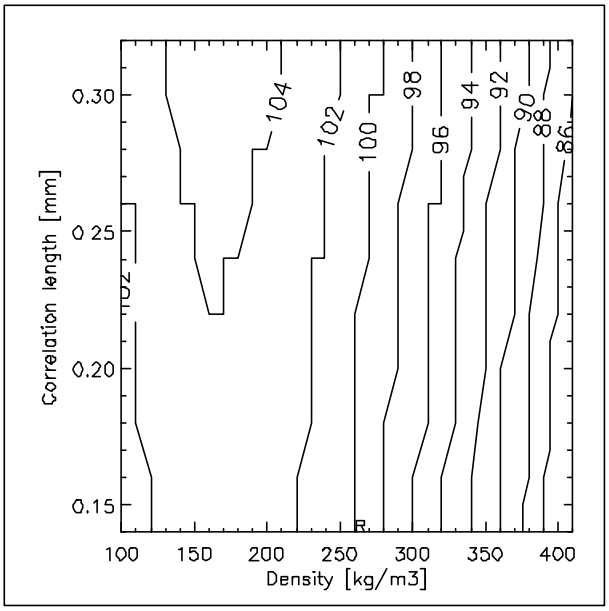

Figure 14. Simulated Comiso Boot-strap algorithm (polarisation mode) sensitivity to variations in layering and grain size in the snow cover.

5.3.7. NORSEX algorithm

The NORSEX algorithm uses an iterative approach to correct for both surface temperature and atmospheric opacity before using Tb_{19v} and Tb_{37v} for computing the ice concentration. Its sensitivity to density of the upper snow layer and correlation length of the bottom snow layer is shown in

figure 15.

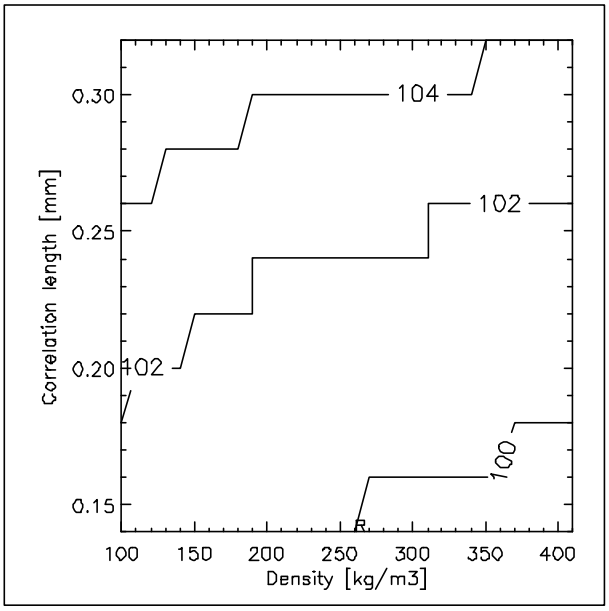

Figure 15. Simulated NORSEX algorithm sensitivity to variations in layering and grain size in the snow cover.

5.3.8. TUD algorithm

The TUD algorithm makes use of the high frequency polarisation difference to improve the resolution of the Boot-strap algorithm (frequency mode) ice concentration estimate. Its sensitivity to density of the upper snow layer and the correlation length of the bottom snow layer is shown in figure 16.

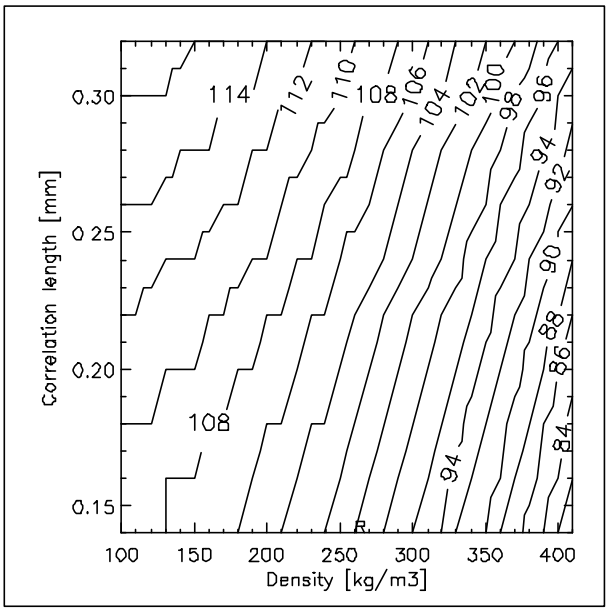

Figure 16. Simulated TUD algorithm sensitivity to variations in layering and grain size in the snow cover.

5.3.9. NASA Team2

The NASA Team2 algorithm makes use of the high frequency polarisation ratio to minimize the sensitivity to the variable surface emissivity that is observed in the NASA Team algorithm. By

applying rotations to the (PR_{19},$GR_{19v/37V}$) and (PR_{85},$GR_{19V/37V}$) domains ice type dependencies are eliminated and in all three parameters are thus defined:

$$\begin{aligned}
\Delta GR &= GR(19,85,H) - GR(19,85,V) \\
PR_R(19) &= -GR(19,37,V)\sin f_{19} + PR(19)\cos f_{19} \\
PR_R(85) &= -GR(19,37,V)\sin f_{85} + PR(85)\cos f_{85}
\end{aligned} \qquad (3)$$

Moreover, the above mentioned surface effects primarily affect ΔGR and $PR_R(19)$, leaving $PR_R(85)$ practically unaffected. First-year (type A) and multiyear ice (type B) are indistinguishable in this parameter space, while ice affected by surface effects now forms an independent surface type (type C). To allow a correction for the atmospheric contamination, $PR_R(19)$, $PR_R(85)$ and ΔGR are modelled by radiative transfer modelling. These parameters, simulated by MEMLS, are shown in figure 19 and 20. The model ice concentration is varied from 0 to 100 % in steps of 1 % for 12 different atmospheric states (6 cloud configurations, 2 seasons). Ice concentration in this respect is the fractional coverage of both type A/B and type C, thus the resulting set of simulated data has three input dimensions. This simulated data is used as a look-up table to compute a penalty function summing the squares of the residuals with respect to the measured values, which is minimised to yield estimates of ice concentration (type A/B and type C) and the best fit atmospheric state.

Since tie-points are specified implicitly in the above mentioned look-up tables, the adaptation to the model data was performed by deriving a constant offset between reference simulated brightness temperatures and the brightness temperatures of the NASA Team2 clear winter model atmosphere over first-year ice. This offset was subtracted from all simulated brightness temperatures prior to calculation of ice concentration.

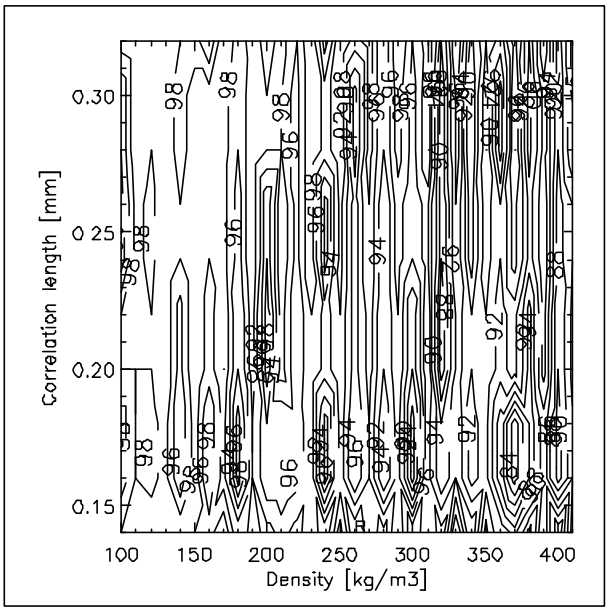

Figure 17. Simulated NASA Team2 algorithm sensitivity to variations in layering and grain size in the snow cover.

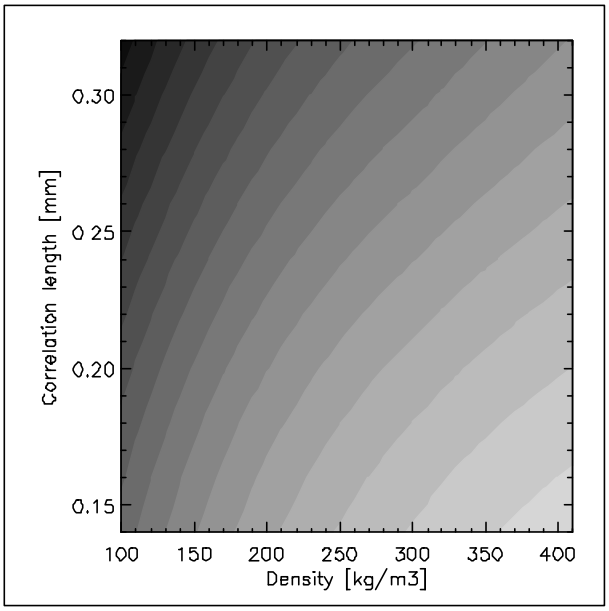

Figure 18. Simulated $GR_{37v/89v}$ sensitivity to variations in layering and correlation length of the snow cover.

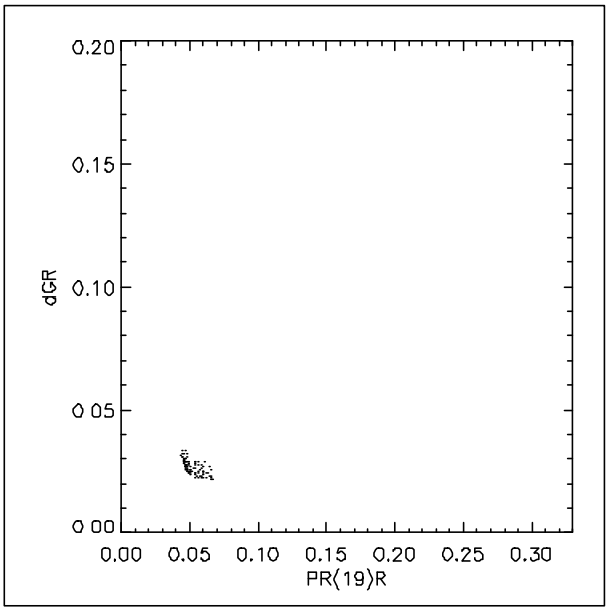

Figure 19. Simulated ΔGR versus PR(19)R.

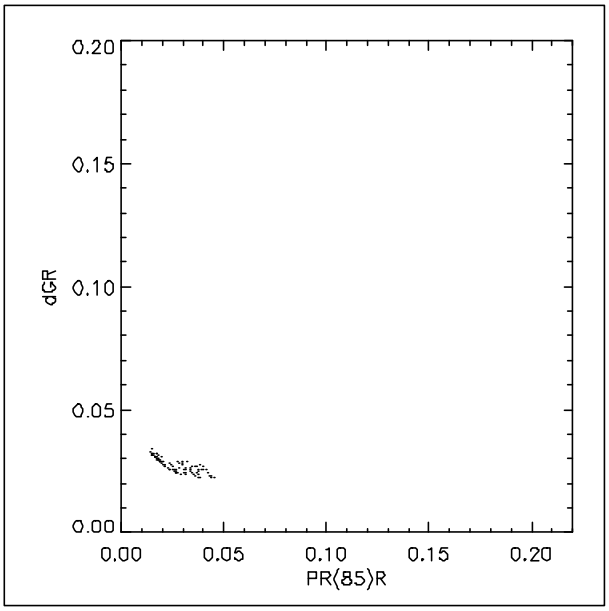

Figure 20. Simulated versus PR(89)R.

Figures 19 and 20 in comparison to Figure 2 of Markus & Cavalieri (2000) show that the MEMLS simulated emissivities tend to mimic weather influence rather than follow the locus from ice type A/B to ice type C.

6. Discussion of simulation results

For a given frequency the dielectric constant ($e = e' - ie''$) (and refractive index) of dry snow is a function of density. The reflection and transmission coefficients between air and snow and between layers with different density within the snow pack is therefore also a function of snow density. The absorption coefficient is a function of the dielectric loss (e'') of the snow and ice. Scattering is a function of correlation length (measure of scatter size and distribution). By changing the upper layer snow density and the correlation length of the bottom snow layer within realistic/ natural ranges in the profile described in table 4, MEMLS simulates significant changes of the snow-ice emissivity and brightness temperature. These simulations investigate sensitivity to snow pack layering and snow grain size enlargements, which are believed to be common consequences of temporary warming and general snow pack metamorphosis (Tonboe et al., 2003). It is a virtue for ice concentration algorithms to compute the ice concentration without sensitivity to changes in the surface emissivity because anomalous surface emissivity is difficult or impossible to correct before comp utation of the ice concentration. The MEMLS simulations of ice concentration, shown in section 4.2, indicate, never the less, that some algorithms are sensitive to the simulated changes in the snow/ice emissivity. As expected, the polarisation difference or ratio is sensitive primarily to density contrasts and the spectral gradient is sensitive to correlation length (grain size).

6.1. The validity of MEMLS for sea ice emissivity simulations

Validation of this extended version of MEMLS for sea ice requires coincident precise vertical profile measurement of the central snow and ice parameters (density, correlation length, temperature, salinity) and surface mounted radiometer measurements at the relevant frequencies. These measurements have not been available to us and in a strict sense, it has therefore been impossible to conduct a validation of MEMLS for sea ice. MEMLS is however, a state-of-the art model and it has been validated and tested for snow cover on land.

In section 4.1 we show a comparison between coincident *in situ* snow and ice measurements and satellite AMSR measurements for two profiles. The simulations using the *in situ* data and AMSR data only match at some frequencies and polarisations. However, the very different snow profiles on a first-year ice floe measured at two points with little horizontal spacing indicate that it is impossible to extrapolate properties measured in a point to areas covered by the AMSR footprint (5-56km). The comparison in section 4.1 makes little sense.

The AMSR measurements includes in addition to the surface Tb also scattering and radiation from the atmosphere. The atmospheric contribution is not simulated in MEMLS. However, model simulations indicate that cloud liquid water raise Tb, decrease PR_{19} and increase GR_{1937}. Water vapour further decreases PR_{19} (Oelke, 1997).

6.2. Radiometer algorithm ice concentration sensitivity

The nine different algorithms and the results of the ice concentration sensitivity study in section 4 are discussed below.

6.2.1. NASA Team ice concentration sensitivity

In figure 7 we see that $GR_{19/37}$ is largely sensitive to increasing correlation length while PR_{19} is sensitive to the density changes of the upper snow layer. $GR_{19/37}$ largely determines the ratio between first- and multi-year ice concentrations while the concentration of these two ice types is determined by PR_{19}. The simulations show that total NASA Team ice concentration decrease (below 100) as the density contrast between the upper and middle snow layer decrease. At the same time, the dielectric contrast between air and the snow surface and absorption in the upper snow

layer increase. The total concentration in figure 6 is sensitive to changes in the upper snow layer density, while being robust to changes in the bottom snow layer correlation length. The ratio between multi-year/first-year ice concentration (not shown) is in fact sensitive to the correlation length, while the total concentration is robust. The sensitivity of PR_{19} to the changes in the upper snow layer density is then critical for the total NASA Team ice concentration sensitivity to the surface emissivity.

6.2.2. Comiso Boot-strap (frequency mode) ice concentration sensitivity

The sensitivity of the Boot-strap (frequency mode) ice concentration is among the lowest of the nine algorithms to the simulated changes in snow/ice emissivity. The ice concentration increase from about 100% to 104% primarily within the range of correlation lengths. Figure 9 show that the simulated Tb_{19v} and Tb_{37v} is an elongated cluster concentrated along a straight line.

6.2.3. Near 90GHz ice concentration sensitivity

The sensitivity of the Near 90GHz ice concentration estimate is the highest among the 9 algorithms to the simulated changes in snow/ice emissivity. The ice concentration decrease from about 120% to 70% primarily within the range of density in the upper snow layer. The polarisation difference between v and h polarisations at 89 GHz show the same type of sensitivity as the ice concentration. Simulations (not shown) using an infinite snow layer (dielectric half-space) show that the polarisation ratio and difference is sensitive to the air/snow dielectric contrast, i.e. density of the surface snow layer. For low density snow (150kg/m^3) the polarisation difference is minimal. For high density snow (450kg/m^3) the polarisation difference is significant at frequencies between 1-100 GHz.

6.2.4. Bristol ice concentration sensitivity

The inclusion of Tb_{37h} makes the Bristol algorithm more sensitive to the density of the upper snow layer than the Comiso Boot-strap in frequency mode. The sensitivity to the correlation length is about the same as Boot-strap.

6.2.5. Cal-val ice concentration sensitivity

The Cal-val algorithm ice concentration is primarily sensitive to variable surface temperature. In these simulations the surface temperature is constant and its sensitivity to density and correlation length is among the lowest of the 9 algorithms.

6.2.6. Comiso Boot-strap (polarisation mode) ice concentration sensitivity

Since the polarisation ratio is sensitive to variations in density of the upper snow layer (and this algorithm uses the Tb polarisation at 37GHz) the Comiso Boot-strap (polarisation mode) algorithm is also sensitive to this snow parameter.

6.2.7. NORSEX ice concentration sensitivity

The NORSEX algorithm is using the same channels (Tb_{19v} and Tb_{37v}) as the Boot-strap in frequency mode and its simulated sensitivity to the changes in the snow cover properties is similar to Boot-strap. The special feature of NORSEX is primarily to decrease sensitivity to atmospheric opacity in support of the tiepoints.

6.2.8. TUD ice concentration sensitivity

The simulated sensitivity of TUD, using both high (89GHz) and medium-low (19, 37GHz) frequency channels, to the snow cover emissivity is lower than the Near 90GHz algorithm, using only the high frequency channel polarisation. Its sensitivity is, however, second highest among the 9 algorithms.

6.2.9. NASA Team2 ice concentration sensitivity

The complexity of the NASA Team2 algorithm makes interpretation of its sensitivity to the simulated snow cover emissivity variations difficult. We notice that the overall sensitivity is not better than NASA Team. However regions, in terms of density of the upper snow layer and the correlation length of the bottom snow layer, where it fails is distributed in a strange pattern due to the selection of different standard atmospheres (tie-points). The use of near 90GHz channels does not guarantee immunity to the variable surface emissivity. Further, situations with different surface emissivities does mimic different atmospheric states.

6.3. Simulated sensitivity of gradient and polarisation ratios

The simulated sensitivity of gradient and polarisation ratios (PR_7, PR_{19}, PR_{89}, $GR_{7/10}$, $GR_{19/37}$, $GR_{37/89}$) within the snow parameter ranges (see section 4.3) used for the ice algorithm sensitivity studies is shown in figure 21. It is in particular the GR sensitivity that increases as a function of frequency. Note that the high frequency polarisation ratio is at 89GHz, while the medium and low frequency polarisation ratios are using the lower frequency for polarisation ratio (7 and 19GHz).

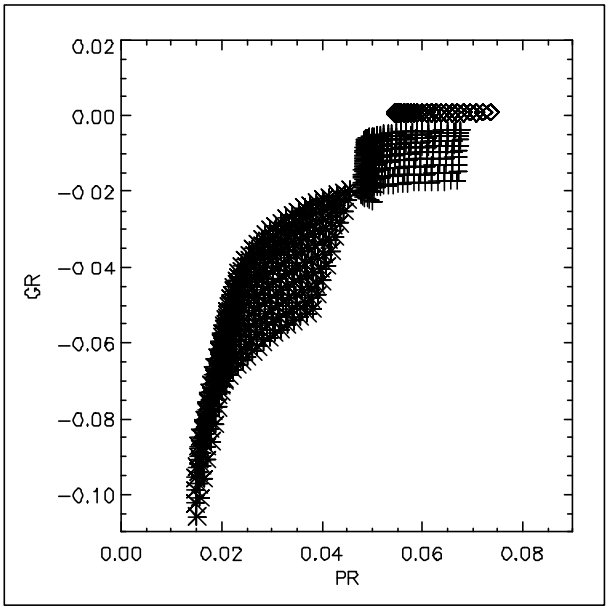

Figure 21. The simulated sensitivity of polarisation and gradient ratios. * = $PR_{89}/GR_{37/89}$, + = $PR_{19}/GR_{19/37}$,<> = $PR_7/GR_{7/10}$.

Especially in the 37-89 GHz range, it is clear that the upper snow cover is determining penetration depth and whether or not the radiometer ever ‘sees’ the structure of the snow layers beneath. Low gradient ratios imply scattering and often deep penetration and this is seen in conjunction with relatively low polarisation ratios. Low polarisation ratios imply a relatively low contrast between the air and snow. The effect is less pronounced in the 19-37 GHz range and not notable in the 7-10 GHz range. The latter is probably mainly caused by the small spectral distance 7 to 10 GHz and the small snow grain size compared with the wavelength (scattering is less significant).

7. Summary of results and future activities

As a step towards completing the second objective in the IOMASA project we have simulated the sensitivity of 9 different radiometer ice concentration algorithms to emissivity changes of the sea ice snow cover using the microwave emission model MEMLS. The simulated sensitivity of each of the 9 algorithms to two central snow properties (density of the upper snow-layer and correlation length of the bottom snow layer) is rated in table 5.

Algorithm	**Density**	**Correlation length**
NASA Team	**Medium/high**	*Low*
Boot-strap frequency mode	*Low*	*Low*
Near 90GHz	**High**	**Medium/high**
Bristol	Medium	*Low*
Cal-val	*Low*	*Low*
Boot-strap polarisation mode	**High**	*Low*
NORSEX	*Low*	*Low*
TUD	**High**	Medium
NASA Team2	**Medium/high**	Medium

Table 5. Rating of algorithms total concentration sensitivity [*low* (<5%)/ medium (5-10%)/ **high** (>10%)] in terms of upper snow layer density and bottom snow layer correlation length.

The choice of channels used in the algorithms determines the performance of the algorithm. Therefore the Boot-strap frequency mode, Cal-val and NORSEX yield virtually identical results. Considering that, these algorithms have similar sensitivities to atmospheric opacity; they can be regarded identical in all practical applications (Andersen et al., 2003).

The combination of Tb_{19v} and Tb_{37v} like in the Comiso boot-strap algorithm in frequency mode, NORSEX and Cal-val has low sensitivity to the simulated emissivity changes. Algorithms also using Tb_{37h} like Bristol, NASA Team and Boot-strap in polarisation mode are sensitive to the simulated density of the upper snow layer. The simulated high sensitivity of the 89GHz polarisation difference to both density and correlation length makes the algorithms using the high frequency channel like Near 90GHz and TUD very sensitive to the simulated snow cover emissivity.

Mätzler et al. (1984) reported results from a field experiment that the high frequency (94 GHz) polarisation difference appeared insensitive to ice lenses at 7 cm depth in the snow. This observation was explained by strong attenuation and isotropic scattering in the upper snow layer (Mätzler et al., 1984). They further noted that *"… at 94 GHz the surface reflectivity will lead primarily to polarization effects …* "(Mätzler et al., 1984, p. 335). The shallow penetration of the near 90 GHz microwaves (confined to the upper centimetres of the snow cover) means that different ice types with snow cover has similar radiative signatures. Further, that ice lenses below the upper centimetres snow are only vaguely affecting the near 90 GHz emissivity. In other words, the near 90GHz emissivity is largely insensitive to ice type and ice layers within the snow-pack, which are affecting and complicating the interpretation of emissivity at e.g. 19 and 37GHz. These observations lead to the development of the Near 90 GHz ice concentration algorithm that exploits the higher spatial resolution at this frequency (Svensden et al., 1987).

However, the near 90 GHz polarisation difference is indeed sensitive to snow-ice surface emissivity and this model experiment indicate that the polarisation difference (at 89GHz) increase as a function of air-snow dielectric contrast/ reflectivity (upper snow layer density). The air-snow density contrast was not explicitly the theme of the laboratory experiment of Barber et al. (1998). Even so, they note that as the dielectric constant of the snow layer increase the 90GHz emissivity at horizon-

tal polarisation decrease while the vertical polarisation is stable. This confirms our model experiments.

The interpretation of NASA Team2 algorithm sensitivity was rather perplexing. The different snow/ice emissivity situations mimic different atmospheric states and thereby standard atmospheres (atmospheric correction/ tie-point set). This makes the sensitivity in terms of the two snow properties erratic.

Validation of MEMLS for sea ice is of significant importance for confidence in the simulation results. However, we note that only snow properties are changed during the simulations and that MEMLS has been validated for snow on land. The latter and the rather successful simulation results give expectations of a successful future validation of MEMLS for sea ice.

We plan to investigate the low-frequency (7 and 10GHz) of AMSR using MEMLS. The investigation will search for low-frequency channel combinations with low sensitivity to changes of the surface emissivity.

The focus of this investigation has been on simulations changing two snow cover properties (density and correlation length). The possible constellations are numerous and in future other parameters can be investigated or cases can be used as reference. It is clear that the field data available so far have limited usefulness. In particular, it would be desirable to obtain field emissivity measurements together with a thorough quantitative description of the ice and snow. In view of the critical dependence of the scattering parameterisation at 89 GHz, field measurements at this frequency are essential tools to obtain a correct model setup. This study aimed at showing that simulation of sea ice emissivity is possible using this extended version of MEMLS. Further, these simulations help in selecting a successful ice concentration algorithm in IOMASA.

Glossary

AMSR	Advanced Microwave Scanning Radiometer
CRYOVEX	CRYOsat Validation Experiment, Fram Strait 2003.
EM	Electro-Magnetic
FY	First-Year (ice)
GR	Gradient Ratio
IOMASA	Integrated Observing and Modelling of the Arctic Sea ice and Atmosphere, EU 5th framework programme project.
MEMLS	Microwave Emission Model for Layered Snow-packs
MY	Multi-Year (ice)
PR	Polarisation Ratio
SSM/I	Special Sensor Microwave Imager, radiometer onboard DMSP.
Tb	Brightness temperature

References

Andersen, S. (1999) Monthly Arctic sea ice signatures for use in passive microwave algorithms. Proc. EUMETSAT Meteorological Data Users Conference, 6-10 September 1999, Copenhagen

Andersen, S., S. Kern & H. Schyberg (2003). Improved retrieval of sea ice total concentration from spaceborne passive microwave observations using numerical weather prediction model fields. Submitted to *Remote Sensing of Environment*.

Barber, D. G. A. K. Fung, T. C. Grenfell, S. V. Nghiem, R. G. Onstott, V. I. Lytle, D. K. Perovich & A. J. Gow (1998). The role of snow on microwave emission and scattering over first-year sea ice. *IEEE Transactions on Geoscience and Remote Sensing 36*(5), 1750-1763.

Belchansky, G. I., & D. C. Douglas (2002). Seasonal comparisons of sea ice concentration estimates derived from SSM/I, OKEAN, and RADARSAT data. *Remote Sensing of Environment 81*, 67-81.

Cavalieri, D.J, P. Gloersen, & W. J. Cambell (1984). Determination of sea ice parameters with the NIMBUS 7 SMMR. *Journal of Geophysical Research 89*(D4), 5355-5369.

Comiso, J.C. (1986). Characteristics of arctic winter sea ice from satellite multispectral microwave observations. *Journal of Geophysical Research 91*(C1), 975-994.

Comiso, J.C., D. J. Cavalieri, C. L. Parkinson, & P. Gloersen (1997). Passive microwave algorithms for sea ice concentration: a comparison of two techniques. *Remote Sensing of Environment 60*, 357-384.

Emery, W. J., C. Fowler, & J. Maslanik (1994). Arctic sea ice concentrations from special sensor microwave imager and advanced very high resolution radiometer satellite data. *Journal of Geophysical Research 99*(C9), 18329-18342.

Fuhrhop, R. T. Grenfell, G. Heygster, K-P. Johnsen, P. Schlüssel, M. Schrader & C. Simmer (1998). A Combined Radiative Transfer Model for Sea Ice, Open Ocean and Atmosphere. *Radio Science 33*(2), pp. 303-316.

Fuhrhop, R., C. Simmer, M. Schrader, G. Heygster, K.-P. Johnsen, P. Schlüssel (1997). Study of passive remote sensing of the atmosphere and surface ice. Berichte aus dem Inst. für Meereskunde an der Christian-Albrechts- Universität Kiel nr. 297.

Johnsen, K.-P. & G. Heygster (2000). Interference Effects in Freshwater and Sea Ice. In: C. Mätzler, COST Action 712, Radiative Transfer Models for Microwave Radiometry, Final Report (pp. 149-162). European Comission, EUR 19543 EN.

Markus, T.; Cavalieri, D.J. (2000) An enhancement of the NASA Team sea ice algorithm. *IEEE Transactions on. Geoscience. and Remote. Sensing., 38*(, 3), 1387-1398

Mätzler, C. (1987). Applications of the Interaction of Microwaves with the natural Snow Cover. *Remote Sensing Reviews 2*(2), pp. 259-391.

Mätzler, C. (1998). Improved Born approximation for scattering of radiation in a granular medium. *Journal of Applied Physics 83*(11), 6111-6117.

Mätzler, C. (2002). Relation between grain size and correlation length of snow. *AGU fall meeting, San Francisco, USA.Journal of Glaciology 48*(162), 461-466.

Mätzler, C., R. O. Ramseier and E. Svendsen (1984). Polarisation effects in sea ice signatures. *IEEE Journal of Oceanic Engineering OE-9*(5), 333-338.

Moritz, R. E. (1988). The ice budget of the Greenland Sea. (Ph.D. thesis) University of Washington technical report APL-UW TR8812.

Oelke, C. (1997). Atmospheric signatures in sea-ice concentration estimates from passive microwaves: modelled and observed. *International Journal of Remote Sensing 18*(5), 1113-1136.

Pedersen, L.T. (1998) Chapter 6.2 in Sandven et al. *IMSI report no. 8. Development of new satellite ice data products* (Chapter 6.2). Bergen, Norway: NERSC Technical Report no. 145, Nansen Environmental and Remote Sensing Center

Ramseier R.O. (1991) Sea ice validation. In J.P. Hollinger (ed.), *DMSP special sensor micro-*

wave/imager calibration/validation - Final report volume II, Washington, DC: Naval Research Laboratory

Shokr, M. E. (1998). Field Observations and model calculations of dielectric properties of Arctic sea ice in the microwave C-band. *IEEE transactions on Geoscience and Remote Sensing 36*(2), 463-478.

Smith, D.M. (1996) Extraction of winter sea-ice concentration in the Greenland and Barents Seas from SSM/I data. *International. Journal of. Remote. Sensing., 17*(, 13), 2625-2646.

Steffen, K., & A. Schweiger (1991). NASA Team algorithm for sea ice concentration retrieval from Defence Meteorological Satellite Program Special Sensor Microwave Imager: comparison with Landsat satellite imagery. *Journal of Geophysical Research 96*(C12), 21971-21987.

Stiles, W. H. & F. T. Ulaby (1980). The Active and Passive Microwave Response to Snow Parameters 1. Wetness. *Journal of Geophysical Research 85*(C2), 1037-1044.

Stogryn, A. (1986). A study of the Microwave Brightness Temperature of Snow from the Point of View of Strong Fluctuation Theory. *IEEE Transactions on Geoscience and Remote Sensing 24*(2), pp. 220-231.

Surdyk, S. & M. Fily (1993). Comparison of the passive microwave spectral signature of the Antarctic ice sheet with ground traverse data. *Annals of Glaciology 17*, 161-166.

Svendsen, E., C. Mätzler, & T.C. Grenfell (1987). A model for retrieving total sea ice concentration from spaceborne dual-polarized passive microwave instrument operating near 90 GHz. *International Journal of Remote Sensing 8*(10), 1 479-1 487.

Svendsen, E.; Kloster, K.; Farelly, B.; Johannesen, O.M.; Johannesen, J.A.; Campbell, W.J.; Gloersen, P.; Cavalieri, D.J.; Mätzler, C. (1983) Norwegian remote sensing experiment: Evaluation of the Nimbus 7 scanning multichannel microwave radiometer for sea ice research. *Jjournal of. Geophysical Research., 88*, (C5), 2781-2791

Tonboe, R., S. Andersen & L. Toudal (2003). Anomalous winter sea ice backscatter and brightness temperature. *Danish Meteorological Institute Scientific Report 03-13*, pp. 59.

Ulaby, F. T., R. K. Moore & A. K. Fung (1986). *Microwave Remote Sensing, From Theory to Applications, vol. 3.* Dedham MA: Artech House.

Wiesmann, A. & C. Mätzler (1999). Microwave emission model of layered snowpacks. *Remote Sensing of Environment 70*, 307-316.

Winebrenner, D. P., J. Bredow, A. K. Fung, M. R. Drinkwater, S. Nghiem, A. J. Gow, D. K. Perowich, T. C. Grenfell, H. C. Han, J. A. Kong, J. K. Lee, S. Mudaliar, R. G. Onstott, L. Tsang, R. D. West (1992). Microwave Sea Ice Signature Modelling. In: F. D. Carsey (Ed.). *Microwave remote sensing of sea ice, Geophysical monograph 68* (pp. 137-175). Washington DC: American Geophysical Union.

Previous reports

Previous reports from the Danish Meteorological Institute can be found on:
http://www.dmi.dk/dmi/dmi-publikationer.htm